Mechanics Research Communications 79 (2017) 15–23

Contents lists available at ScienceDirect

Mechanics Research Communications

journal homepage: www.elsevier.com/locate/mechrescom

Two-fluid smoothed particle hydrodynamics simulation of submerged granular column collapse

Chun Wang [a,*], Yongqi Wang [b,*], Chong Peng [c], Xiannan Meng [b]

[a] Collaborative Innovation Center for Advanced Ship and Deep-Sea Exploration, School of Naval Architecture, Ocean and Civil Engineering, Shanghai Jiao Tong University, 800 Dongchuan Road, Shanghai 200240, PR China
[b] Chair of Fluid Dynamics, Department of Mechanical Engineering, Technische Universität Darmstadt, Otto-Berndt-Str. 2, 64287 Darmstadt, Germany
[c] Institute of Geotechnical Engineering (IGT), Universitaet fuer Bodenkultur, Feistmantelstrasse 4, 1180 Vienna, Austria

ARTICLE INFO

Article history:
Received 16 June 2016
Received in revised form 8 September 2016
Accepted 2 December 2016
Available online 7 December 2016

Keywords:
Submerged granular column collapse
Water–granular mixture flow
SPH method
Numerical simulation

ABSTRACT

In this paper, a two-fluid smoothed particle hydrodynamics (SPH) model, based on the mixture theory, is employed to investigate the complex interactions between the solid particles and the ambient water during the process of submerged granular column collapse. From the simulation, two regimes of the collapse, one being quick and the other being slow, are identified and the reasons of formation are analyzed. It is found that, a large internal friction angle of the granular phase, representing large drag force between solid particles, helps form the slow regime. Small hydraulic conductivity, representing large inter-phase drag force, also retards the collapse dramatically. Good agreements between our numerical results and other researchers' numerical and experimental results are observed, which demonstrates the capability of the proposed two-fluid SPH approach in dealing with saturated water–soil mixture flows.

1. Introduction

Submerged soil column collapse is a typical water–soil interaction problem and a model for many underwater natural and hazardous processes, such as debris flows [1], landslides [2], submarine avalanches [3], to name but a few. Due to its harmful impacts to the safety of the underwater structures or the geomorphology changing of waterways, submerged granular column collapse has long been a research concern for geophysicists, hydrologists and underwater engineers. There are a large amount of experimental and numerical works dealing with the dry granular flows (such as sand, glass beads, etc.); among them, the so-called $\mu(I)$-rheology [4,5] has recently emerged as a major step toward consistently describing the granular materials. Lagree et al. [6] implemented the $\mu(I)$-rheology in a Navier–Stokes solver and simulated the unsteady 2D collapse of granular columns over a wide range of aspect ratios. Ionescu et al. [7] proposed a $\mu(I)$-rheological numerical model for dry granular column collapse over inclined planes.

Compared to dry soil column collapse, however, the process of submerged soil column collapse has not yet been well understood, due to the complex interactions between water and solid particles. For better understanding of the challenges and the recent developments on this topic, readers may refer to Rondon et al. [8], Meruane et al. [9,10], Savage et al. [11] and the references therein.

During the collapse process, soil undergoes large deformation which is difficult to treat using grid-based methods. Problems that involve history-dependent constitutive models, like large deformation plasticity, are expressed more naturally in a Lagrangian computational frame. For this reason, meshfree Lagrangian particle methods for soil mechanics seem to be increasing in popularity recently.

Bui et al. [12] conducted the numerical simulation of the waterjet–soil interactions using the smoothed particle hydrodynamics (SPH) method which is a fully Lagrangian and meshfree method. They proposed a two-phase model, in which the water is regarded as a Newtonian fluid and the soil as an elastic-perfectly plastic material. Interactions between water and soil were modeled by the Darcy's law and pore water pressure. With the aid of this novel numerical method, some interesting phenomena in water–soil interactions have been revealed. Bui et al. [13] and Bui and Fukagawa [14] proposed an incremental plasticity model to describe the large deformation behavior of soil. Recently, authors of this paper (see [15]) developed an SPH approach for large deformation analysis with hypoplastic constitutive model. Dunatunga and Kamrin [16] developed a material point method (MPM) to simulate dry granular flows with $\mu(I)$ inertial rheology. In Zhang et al. [17], a

* Corresponding authors.
E-mail addresses: chunwang@sjtu.edu.cn (C. Wang), wang@fdy.tu-darmstadt.de (Y. Wang).

http://dx.doi.org/10.1016/j.mechrescom.2016.12.001
0093-6413/

version of the particle finite element method (PFEM) was proposed to analyze the large deformation of granular flow problems.

More recently, we proposed a two-fluid SPH mixture model to analyze the waterjet–soil interaction problem [18–20]. In this model, each constituent of the mixture satisfies its own conservation equations of mass and momentum. Unlike Bui et al. [12], volume fractions of both constituents are taken as field variables which must be determined together with the other fundamental variables, such as pressure and velocities. With this mixture model, it is possible to investigate the temporal and spatial evolutions of the volume fractions of both constituents.

In this paper, the proposed two-fluid SPH mixture model is employed to analyze the water–soil interactions during submerged granular column collapse. Two regimes of the collapse, one is quick and the other is slow, could be observed from the simulations. Key factors influencing the formation of different regimes, namely the internal friction angle and the hydraulic conductivity of the soil, are investigated, which helps reveal the mechanisms of soil failure in the presence of an ambient fluid.

2. Mathematical formulation

2.1. Water–soil mixture model

The role of the ambient fluid can be investigated through a two-phase continuum mixture theory (e.g. [9,18,21]). Mixture theory assumes that, at any time, every point in space is occupied simultaneously by one particle of each constituent. With this assumption, we can define partial densities ρ_η, partial velocities $\boldsymbol{v}_\eta$, and partial stresses $\boldsymbol{\sigma}_\eta$ for each constituent. Here $\eta = l, s$ for fluid and solid, respectively. Each constituent must satisfy individual balance laws for the conservation of mass

$$\frac{\mathrm{D}^\eta \rho_\eta}{\mathrm{D}t} = -\rho_\eta \nabla \cdot \boldsymbol{v}_\eta, \tag{1}$$

and momentum

$$\rho_\eta \frac{\mathrm{D}^\eta \boldsymbol{v}_\eta}{\mathrm{D}t} = \nabla \cdot \boldsymbol{\sigma}_\eta + \rho_\eta \boldsymbol{g} + \boldsymbol{f}_\eta, \tag{2}$$

where $\boldsymbol{g}$ the gravitational acceleration, and $\mathrm{D}^\eta(\cdot)/\mathrm{D}t$ the material time derivative along the path of particles of η phase. The interaction force $\boldsymbol{f}_\eta$ is the force exerted on phase η by the other constituent. By definition, the sum over the two constituents is equal to zero, i.e. $\boldsymbol{f}_l + \boldsymbol{f}_s = 0$.

In mixture theory we should specify how partial variables are related to their physical, or intrinsic, counterparts. In standard mixture theory, the partial and intrinsic velocity fields are identical, while the densities are related by volume fractions, i.e.

$$\rho_\eta = \phi_\eta \tilde{\rho}_\eta, \quad \boldsymbol{v}_\eta = \tilde{\boldsymbol{v}}_\eta, \tag{3}$$

where variables with a tilde denote intrinsic variables, and ϕ_η is the volume fraction of phase η, satisfying $\phi_l + \phi_s = 1$ for a saturated liquid-solid mixture.

For the soil stress, we assume that

$$\boldsymbol{\sigma}_s = \phi_s \tilde{\boldsymbol{\sigma}}_s, \quad \boldsymbol{\sigma}_l = -p\boldsymbol{I} + \phi_l \tilde{\boldsymbol{\tau}}_l, \tag{4}$$

where $\tilde{\boldsymbol{\sigma}}_s$ is the intrinsic stress of the soil, p the pore water pressure, and $\tilde{\boldsymbol{\tau}}_l$ the intrinsic deviatoric stress tensor of the water. The interaction force $\boldsymbol{f}_s$ (i.e. $-\boldsymbol{f}_l$) is assumed to be in the form

$$\boldsymbol{f}_s = -\phi_s \nabla p + C_d(\boldsymbol{v}_l - \boldsymbol{v}_s). \tag{5}$$

Here the second term on the right-hand side is simply an interphase resistance term, with C_d being the drag coefficient. The first term can be identified as a buoyancy force, e.g. the surface pressure exerted across the surface of the solids because of the surrounding fluid. The buoyancy force, combining with $-\nabla p$ in the momentum balance equation of water, leaves $-\phi_l \nabla p$. This ensures, as in Darcy's law, that the percolation process is driven by intrinsic (pore) rather than partial pressure gradients (e.g. [22]).

In the current study, the so-called weakly compressible SPH (WCSPH) method is employed to investigate the fluid dynamics. In WCSPH, the pressure is given by the equation of state of water, in such a manner that the fluctuation of the water density is less than 1% which represents a very weak compressibility. For the SPH method, mass conservation is always assured, because the mass of each particle is fixed and the number of particles remains unchanged during the simulation.

The constitutive relationship and equation of state for water can be seen in Wang et al. [18]. Here we only give a brief description on the constitutive relationship of the soil and the interaction model between water and soil.

2.2. Constitutive laws of soil and interaction forces

In this study, the intrinsic density $\tilde{\rho}_s$ of the solid particles is assumed as constant. Consider the soil as an elastic-perfectly plastic material with a Drucker-Prager yield criterion

$$F(I_1, J_2) = \sqrt{J_2} + \alpha_\theta I_1 - k_c, \tag{6}$$

where I_1 is the first invariant of the total stress tensor $\tilde{\sigma}_s^{\alpha\beta}$, and J_2 is the second invariant of the deviatoric stress tensor $\tilde{\tau}_s^{\alpha\beta}$. In Eq. (6), α_θ and k_c are constants which can be related to the cohesion c and the friction angle θ of the Mohr-Coulomb failure criterion by matching the two models [23, p. 149]. In this paper, cohesion is considered as zero, thus $k_c = 0$. For plane strain problem, α_θ is determined by

$$\alpha_\theta = \frac{\tan\theta}{\sqrt{9 + 12\tan^2\theta}}. \tag{7}$$

In computational plasticity theory, it is assumed that the total strain in a body can be decomposed into an elastic part and a plastic part. The elastic part of the strain can be computed from a linear elastic constitutive law, e.g. the Hooke's law. To model the plastic part, however, we need a flow rule which states how the plastic deformation takes place once the stress threshold has been reached. With this decomposition, the total strain rate tensor $\dot{\varepsilon}_s^{\alpha\beta}$ can be written as

$$\dot{\varepsilon}_s^{\alpha\beta} = \frac{\dot{\tilde{\tau}}_s^{\alpha\beta}}{2G} + \frac{1-2\nu}{3E}\dot{\tilde{\sigma}}_s^{\gamma\gamma}\delta^{\alpha\beta} + \dot{\lambda}\frac{\partial H}{\partial \tilde{\sigma}_s^{\alpha\beta}}, \tag{8}$$

where α, β are free indices and γ is a dummy index; $\delta^{\alpha\beta}$ is Kronecker's delta, $\delta^{\alpha\beta} = 1$ if $\alpha = \beta$ and $\delta^{\alpha\beta} = 0$ if $\alpha \neq \beta$; $\tilde{\tau}_s^{\alpha\beta} = \tilde{\sigma}_s^{\alpha\beta} - \frac{1}{3}\tilde{\sigma}_s^{\gamma\gamma}\delta^{\alpha\beta}$ is the deviatoric part of the total stress tensor $\tilde{\sigma}_s^{\alpha\beta}$; G is the shear modulus and ν the Poisson's ratio; $\dot{\lambda}$ is the rate of change of the so-called plastic multiplier λ dependent on the state of stress and load history and H is the plastic potential function.

Rearranging (8), the general stress–strain relationship for an elastic-perfectly plastic material can be derived as

$$\dot{\tilde{\sigma}}_s^{\alpha\beta} = 2G\dot{e}_s^{\alpha\beta} + K\dot{\varepsilon}_s^{\gamma\gamma}\delta^{\alpha\beta} - \dot{\lambda}\left[2G\frac{\partial H}{\partial \tilde{\sigma}^{\alpha\beta}} + \left(K - \frac{2G}{3}\right)\frac{\partial H}{\partial \tilde{\sigma}^{\gamma\gamma}}\delta^{\alpha\beta}\right], \tag{9}$$

where $\dot{e}_s^{\alpha\beta}$ is the deviatoric part of the strain rate tensor $\dot{\varepsilon}_s^{\alpha\beta}$, K the bulk modulus. $\dot{\lambda}$ can be calculated by using the consistency condition which states that the new stress state after loading still satisfies the yield criterion (6), i.e.

$$\mathrm{d}F = \frac{\partial F}{\partial \sigma^{\alpha\beta}}\mathrm{d}\sigma^{\alpha\beta} = \frac{\partial F}{\partial \sigma^{\alpha\beta}}\dot{\sigma}^{\alpha\beta}\mathrm{d}t = 0. \tag{10}$$

In this paper, two types of flow rule are implemented in the simulation. The first one is the so-called associated flow rule, where

the plastic potential function H is chosen to be equal to the yield function F. With this assumption, the constitutive relation for the soil is in the form

$$\dot{\tilde{\sigma}}_s^{\alpha\beta} - \tilde{\sigma}_s^{\alpha\gamma}\dot{\omega}_s^{\beta\gamma} - \tilde{\sigma}_s^{\gamma\beta}\dot{\omega}_s^{\alpha\gamma} = 2G\dot{e}_s^{\alpha\beta} + K\dot{\varepsilon}_s^{\gamma\gamma}\delta^{\alpha\beta} - \dot{\lambda}\left[3\alpha_\theta K\delta^{\alpha\beta} + \frac{G}{\sqrt{J_2}\tilde{\tau}_s^{\alpha\beta}}\right]. \tag{11}$$

Note that the left hand side of (11) has been replaced by the Jaumann rate, in which $\dot{\omega}_s^{\alpha\beta}$ is the rotational rate tensor. The rate of change of plastic multiplier $\dot{\lambda}$ is calculated by

$$\dot{\lambda} = \frac{3\alpha_\theta K\dot{\varepsilon}_s^{\gamma\gamma} + (G/\sqrt{J_2})\tilde{\tau}_s^{\alpha\beta}\dot{\varepsilon}_s^{\alpha\beta}}{9\alpha_\theta^2 K + G}. \tag{12}$$

The second one is the non-associated flow rule, in which the plastic potential function has the form

$$H = \sqrt{J_2} + 3I_1\sin\psi, \tag{13}$$

where ψ is the dilatancy angle. Dilatancy is the volume change observed in granular materials when they are subjected to shear deformations. Dilatancy always takes part in the associated flow rule, whereas this contribution to the non-associated flow rule is optional through the choice of dilatancy angle ψ. A zero dilatancy angle indicates that the material is plastically incompressible. With the non-associated flow rule, the constitutive relationship for soil is

$$\dot{\tilde{\sigma}}_s^{\alpha\beta} - \tilde{\sigma}_s^{\alpha\gamma}\dot{\omega}_s^{\beta\gamma} - \tilde{\sigma}_s^{\gamma\beta}\dot{\omega}_s^{\alpha\gamma} = 2G\dot{e}_s^{\alpha\beta} + K\dot{\varepsilon}_s^{\gamma\gamma}\delta^{\alpha\beta} - \dot{\lambda}\left[9K\sin\psi\delta^{\alpha\beta} + \frac{G}{\sqrt{J_2}\tilde{\tau}_s^{\alpha\beta}}\right], \tag{14}$$

where the rate of change of plastic multiplier $\dot{\lambda}$ is

$$\dot{\lambda} = \frac{3\alpha_\theta K\dot{\varepsilon}_s^{\gamma\gamma} + (G/\sqrt{J_2})\tilde{\tau}_s^{\alpha\beta}\dot{\varepsilon}_s^{\alpha\beta}}{27\alpha_\theta K\sin\psi + G}. \tag{15}$$

Here we point out that, Eqs. (11) and (12) are equivalent to Eqs. (14) and (15), respectively, in case of $k_c = 0$ and $\alpha_\theta = 3\sin\psi$. For instance, when $\theta = 25^\circ$, according to

$$\alpha_\theta = \frac{\tan\theta}{\sqrt{9 + 12\tan^2\theta}} = 3\sin\psi, \tag{16}$$

we have $\psi \approx 2.61^\circ$. Thus the plastic deformation, e.g. dilatancy, calculated with an associated flow rule of $\theta = 25^\circ$ is equivalent to that obtained by a non-associated flow rule with $\psi = 2.61^\circ$.

In this paper, the drag coefficient C_d in (5) can be derived from the Darcy's law as

$$C_d = \frac{\phi_f\gamma_w}{k}, \tag{17}$$

where k is called hydraulic conductivity with the dimensions of velocity $[LT^{-1}]$, $\gamma_w = \rho_f g$ is the specific weight expressed with the partial density ρ_f of the water. k is a constant depending not only on the type of soil but also on the type of fluid (via dynamic viscosity μ) percolating through it.

3. SPH implementation

SPH is now a well-known method, and we assume the reader is rather familiar with its basics. Thus, we will not describe the classical SPH interpolation and operators. For an extensive formulation of the two-fluid mixture SPH model, please see our recent paper (i.e. [18]) and the references therein. In this section, however, we will summarize some modifications used herein. To simplify the SPH equations for the water and soil it is convenient to reserve the subscripts a and b for the water particles, and i and j for the soil particles.

In Monaghan and Kocharyan [24] and Monaghan [25], the pressure term $-\phi_l\nabla p$ in the momentum equation of water is replaced by $-\nabla(\phi_l p) - p\nabla\phi_s$. However, this treatment leads to numerical instability in the calculation of fluid phase. Thus this term is remained as is in the present paper. The SPH approximation for the momentum equation of water is

$$\frac{\mathrm{D}^l v_a^\alpha}{\mathrm{D}t} = -\phi_a\sum_b m_b\left(\frac{p_a}{\rho_a^2} + \frac{p_b}{\rho_b^2} + \Pi_{ab}\right)\frac{\partial W_{ab}}{\partial x_a^\alpha} + \sum_b m_b\left(\frac{\tau_a^{\alpha\beta}\phi_a}{\rho_a^2} + \frac{\tau_b^{\alpha\beta}\phi_b}{\rho_b^2}\right)\frac{\partial W_{ab}}{\partial x_a^\beta} - \sum_i m_i\frac{f_{ia}^\alpha}{\rho_i\rho_a}W_{ia} + g_a^\alpha, \tag{18}$$

where Π_{ab} is the artificial viscosity term added to prevent non-physical penetration of particles (see [26]). W_{ab} is the interpolation kernel function and a Wendland quintic kernel function is chosen in this study.

Volume fraction ϕ_a for a water particle a is calculated according to

$$\phi_a = 1 - \frac{1}{\tilde{\rho}_s}\sum_j m_j W_{aj}, \tag{19}$$

where the summation term gives soil volume fraction ϕ_s at the position of water particle a. Recalling that $\tilde{\rho}_s$ is constant, we obtain

$$\frac{\mathrm{D}^l\phi_a}{\mathrm{D}t} = -\frac{1}{\tilde{\rho}_s}\sum_j m_j v_{aj}^\alpha\frac{\partial W_{aj}}{\partial x_a^\alpha}, \tag{20}$$

which is actually the SPH approximation of the relation $\mathrm{D}^l\phi_l/\mathrm{D}t = -\mathrm{D}^l\phi_s/\mathrm{D}t$. In the current study, both (19) and (20) are used. We find that, on the one hand, Eq. (20) leads to stable calculation; on the other hand it results in a smoothed gradient field of ϕ_a. Thus, every some time steps, we recalculate it using (19). With this re-initialization technique, the calculation is stable, and the large gradient of ϕ_a (if there is) can still be retained satisfactorily.

4. Simulations and results analysis

In this section, we simulate the granular column collapse process using the proposed two-fluid mixture SPH model. Both loose packing and dense packing are considered in order.

As seen in Fig. 1, the rectangular tank contains a column of water-soil mixture which is delimited by a removable gate. The tank is partially filled with water. At $t = 0$, the gate is suddenly removed and the column then collapses. The arrow in Fig. 1 illustrates the removal of the gate at $t = 0$. Although a short time is needed to remove the gate from the tank, this period is so short that

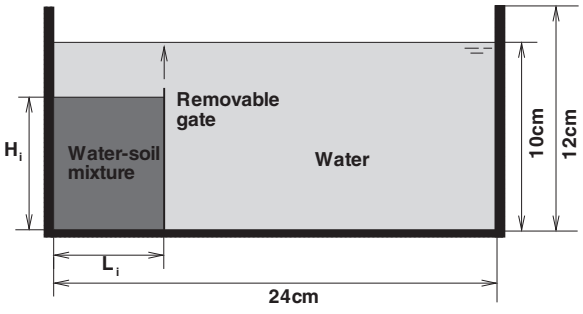

Fig. 1. Submerged granular column collapse.

Table 1
Material properties used in the computation for an initial 6 cm × 8 cm ($L_i \times H_i$) loose packing granular column collapse in water.

Property	Symbol	Value
True density of soil	$\tilde{\rho}_s$	2700 kg/m^3
Young's modulus of soil	E	150 MPa
Poisson's ration of soil	ν	0.3
Internal friction angle of soil	θ	5° and 8°
Initial volume fraction of soil	ϕ_{s0}	0.55
Hydraulic conductivity of soil	k	0.005 m/s
Viscosity of the water	μ	0.012 Pa s
Initial true density of the water	$\tilde{\rho}_{f0}$	1000 kg/m^3

its influence on the collapse can be ignored. Thus in our numerical simulation, the gate is assumed to be removed instantaneously at $t = 0$. The transient removal process is not considered. Further, the initial velocity field immediately after the gate is removed is assumed to be zero.

Material properties used in the calculation are shown in Table 1. The material properties are taken as the same as those provided by Savage et al. [11], except the internal friction angle of the solid phase. The reasoning is given later. In Savage et al. [11], the viscosity of the fluid is 0.012 Pa s, and higher than the viscosity of normal water, i.e. 0.001 Pa s. In fact, we find that the numerical results are not sensitive to the fluid viscosity in particle inertial regime, thus, a typical value for normal water is also possible for the current calculation.

Now we explain why we choose a different value for the internal friction angle. Granular materials are known to change volume when sheared: a dense packing dilates and a loose packing compacts. Critical state theory (e.g. [27]) has pointed out the important role of the dilatancy played in adjusting the friction between solid particles: the dilation of a dense packing ($\psi > 0$) is accompanied by an increase of the apparent friction coefficient, the increase being equal to the dilatancy, whereas the compaction of a loose packing ($\psi < 0$) corresponds to a decrease of the apparent friction. The following equations describe the evolution of the volume fraction and of the shear stress in a granular material subjected to plane-shear at a shear rate $\dot{\gamma}$ under a confining pressure p^s [28]:

$$\frac{1}{\phi}\frac{\mathrm{d}\phi}{\mathrm{d}t} = -\tan\psi\dot{\gamma}, \tag{21}$$

$$\tau^s = \tan\psi p^s + \tau_{eq}, \tag{22}$$

$$\tan\psi = K_3(\phi - \phi_{eq}), \tag{23}$$

where τ_{eq} and ϕ_{eq} are stress and the volume fraction obtained in the steady regime, respectively; K_3 is a constant need to be calibrated. The first equation is a rewriting of the kinematic condition and stipulates how the volume fraction evolves with the strain γ and results from the definition of the dilatancy angle. In fact, from the mass conservation and the definitions of the dilatancy angle ψ and the strain γ, one gets Eq. (21) (see [29, p. 134]). The second equation means that the change in volume fraction implies an additional stress contribution due to the geometrical entanglement. The last equation is a closure relation first proposed by Roux and Radjai [30]. It is obtained by fitting the experimental measurements. It simply assumes that the dilatancy angle is proportional to the difference between the actual volume fraction and the critical volume fraction corresponding to the steady state. Rewriting the second equation as $\tau^s = \tan(\theta + \psi)p^s$, we realize immediately the fact that the dilatancy angle ψ plays the role of adjusting the apparent friction angle θ!

We now make an estimation on the adjustment. As seen in Table 1, the initial solid volume fraction ϕ_{s0} in the present study, is taken as 0.55. According to Rondon et al. [8], it belongs to the loose packing regime. Thus, guided by the critical state theory, a smaller

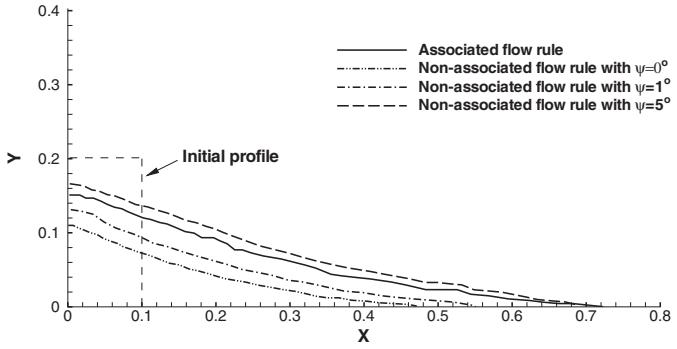

Fig. 2. SPH simulation of dry granular column collapse with associated and non-associated flow rules.

apparent internal friction angle θ should be chosen for the calculation of shear stress. According to Pailha and Pouliquen [27], we choose $\phi_{eq} = 0.60$ and $K_3 = 4.09$. Then from (23) we get $\psi \approx -11.5°$ which is a reduction from the internal friction angle. If the friction angle is about 20°, as in Rondon et al. [8], the reduced apparent friction angle should be about 8.5°. In addition, Rondon et al. [8] pointed out that, for a low initial volume fraction $\phi_{s0} = 0.55$ the final slope is as small as 6.5°, which corresponds to very elongated deposits. Considering these, two apparent fraction angles, e.g. 5° and 8°, respectively, are chosen for the loose packing case.

There are a total of 15,360 fluid particles and 1824 solid particles generated regularly for water and solid phase in the tank, respectively. The initial particle spacing is 0.00125 m. Numerical parameters are chosen as the following: in equation of state of water, $B = 1.4285 \times 10^4$; virtual speed of sound for water $c_f = 10$ m/s; speed of sound for soil $c_s = 215$ m/s; artificial viscosity parameters are taken as $\alpha = 0.1$, $\beta = 0$; the artificial diffusive parameter in δ-SPH method is set as $\delta = 0.1$ for both phases; for the repulsive force, $D = 0.01$ and $r_0 = 0.00125$ m; time step size $\Delta t = 2.5 \times 10^{-6}$ s. For the meaning of the above numerical parameters, please refer to Wang et al. [18].

Fig. 2 shows the dilatancy of dry granular column collapse under the associated and non-associated flow rules, respectively. It is demonstrated that the dilatancy increases with the increase of the dilatancy angle ψ. A dilatancy angle of 5° results an un-physically large swelling of the body, whereas a dilatancy angle of 1° results a moderate swelling. The associated flow rule with an internal friction angle of 25° results in a swelling equivalent to that obtained using non-associated flow rule with a dilatancy angle of 2.61°, as exemplified in Eq. (16). Thus, it is very important to choose a suitable value for the dilatancy angle. For fine-grained soil, the dilatancy angle is normally very small, e.g. less than few degrees. In many simulations, such as in Bui et al. [13], this angle is simply set to zero. Note that, non-associated flow rule with zero dilatancy angle corresponds to plastically incompressible materials, which is also demonstrated in Fig. 2.

Although we have estimated a dilatancy angle of −11.5°, the dilatancy decreases rapidly according to the critical state theory. Thus the dilation of the material is negligible, which is also observed from the experiments of Rondon et al. [8]. In the current study, the non-associated flow rule with a very small dilatancy angle $|\psi| < 0.1°$ is implemented in the calculation.

Numerical simulation shows several interesting characteristics of the submerged granular column collapse. First, waves can be seen at the water surface during the collapse. As shown in Fig. 3, at the initial stage, the sinkage of the column leads to the sinkage of the water surface above. At the meanwhile, free surface at the other end is elevated. Free surface is thus disturbed and waves aroused. Waves propagate back and forth in the tank, affecting the dynamics

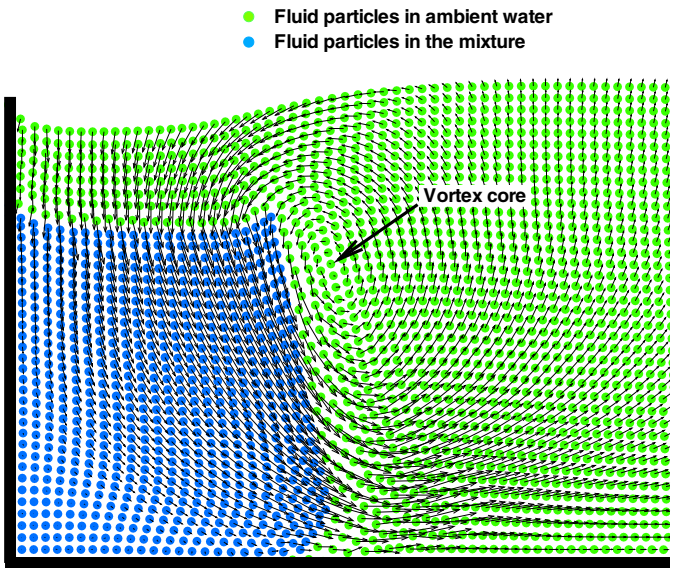

Fig. 3. Velocity field of the fluid at the initial stage of the collapse.

of the collapse. Depending on the wave induced water velocity, the collapse can be accelerated or decelerated.

Second, large vortex can be observed at the initial stage of the collapse. The vortex core is at the upper right corner of the column, as shown in Fig. 3. This vortex is caused by the disturbance of the collapse. During the later stage of the collapse, the vortex propagates and dissipates because of the viscosity of the fluid.

Third, a transition zone of water volume fraction ϕ_f can be found at the interface of the column and the ambient fluid. Fig. 4 shows the values of ϕ_f at some representative times. At the initial stage, e.g. $t=0$, a singular surface exists, where ϕ_f jumps from a lower value in the mixture to its maximum value, i.e. unit, in the ambient fluid. During the collapse, a transition zone of ϕ_f develops, due to the mixing of the solid particles with the ambient fluid. However, we point out that, due to the volume fraction re-initialization technique (i.e. Eq. (19)) used in this study, the transition zone is limited in a narrow space, namely, the abrupt change of the volume fraction at the interface is maintained.

Fig. 5 shows the water pressure field at some representative times. According to the theory of critical state, loose packing material exhibits compaction. As a result of the compaction, the interstitial pore water is squeezed out from the column, giving rise to a positive pore pressure field. Here, "positive" means the pressure is higher than the hydrostatic pressure of the surrounding fluid at the same depth.

Fig. 6 shows the calculated profiles of the deposit at representative times, compared with the experimental observations of Rondon et al. [8] and FEM results of Savage et al. [11]. It can be seen that the particles come to rest in seconds. Thus the collapse belongs to the quick regime. In this regime, both numerical results of SPH and FEM agree well with the experimental observations, except small flaws of the SPH results at the very front of the granular flow, where a blunt head is formed due to the questionable interaction model applied there by the SPH simulation. In fact, at the front of the granular flow, the particle number is very sparse. Thus it might not be suitable for using the Darcy's interaction model there.

Since the effect of the dilatancy (compaction) is to increase (decrease) the apparent friction coefficient, we can, as a primary

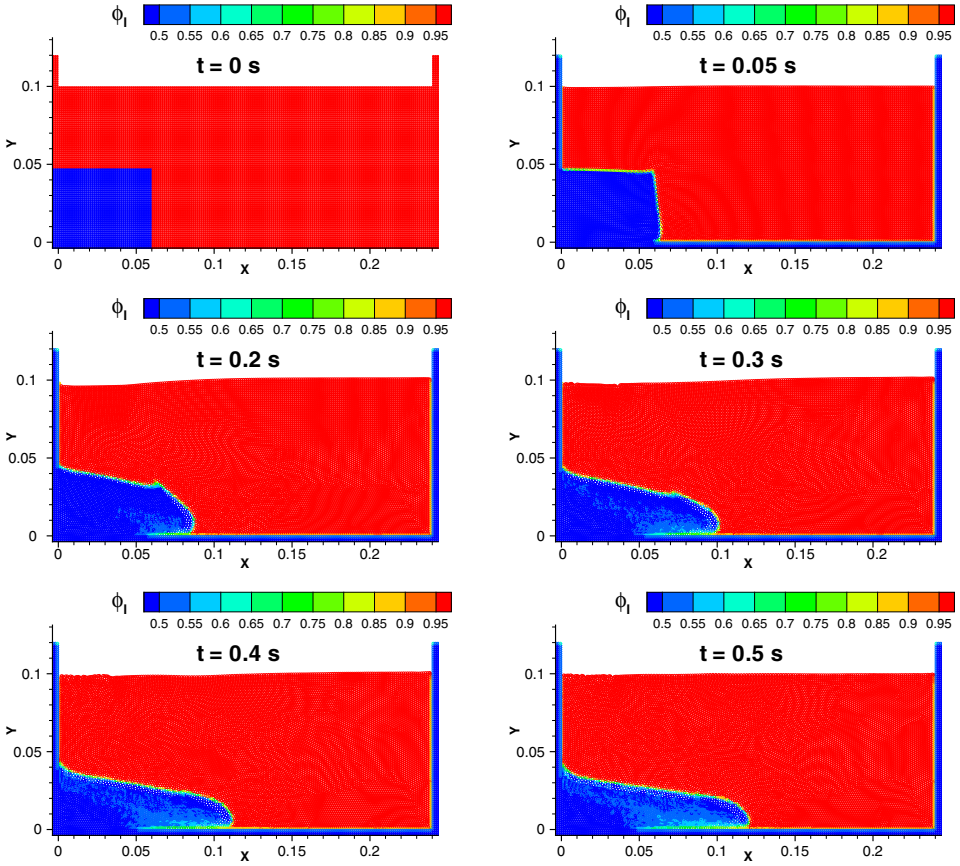

Fig. 4. Water volume fraction ϕ_f at some representative times.

exploration, directly vary the apparent internal friction angle θ to investigate the influence of the dilatancy (compaction) on the dynamics of submerged granular column collapse. Fig. 6 also shows the deposit profiles at a certain time obtained using different apparent frictional angles. We can see that, indeed, the collapse can be retarded by the increase of the frictional angles. In fact, large internal friction angle, representing large drag force between solid particles, yield slow collapse.

Now we come to the dense packing case. Rondon et al. [8] found that the morphology of the deposits is mainly controlled by the initial volume fraction of the granular mass. Initially dense granular columns merely collapse very slowly. For example, a very small increment of the granular volume fraction ϕ_s from 0.55 to 0.60, would drastically increase the collapse time from seconds to tens of seconds! This poses big challenges for numerical modeling. In our simulation of dense granular column collapse, the initial solid volume fraction is set to 0.6, the internal friction angle is set to 25°, while other material parameters are kept the same as in Table 1.

We find that hydraulic conductivity k plays an important role in the dynamics of the mixture flow. Fig. 7 shows the deposit profiles at a certain time obtained for different values of k. We can see that, for low hydraulic conductivity, the collapse is very slow. This is reasonable, because, as we know, hydraulic conductivity depicts whether the fluid can flow through the porous media easily or not. Lower hydraulic conductivity indicates that the fluid can not percolate easily through the granules, leading to a slow collapse. Thus, it is very important to choose an appropriate hydraulic conductivity for the dense granular column collapse. Fig. 8 shows the calculated deposit profile in case of $k = 0.00005$ m/s which is obtained using the following Kozeny–Carman formula [27]

$$k = \frac{K_p \tilde{\rho}_l g}{\mu}, \quad K_p = \alpha d^2, \quad \alpha = \frac{(1-\phi_s)^3}{150\phi_s^2}, \tag{24}$$

for packing of solid spheres of diameter $d = 225$ μm, where K_p is the permeability of the porous media formed by the particles and has the dimensions of a length squared.

From Fig. 8, we can see that our simulation qualitatively reproduces the experimental observations of Rondon et al. [8], except for the upright corner and the front. As in the case of loose packing, the present model is not suitable for predicting the flow front with sparse particles. At the upright corner, our simulation differs from the experimental observations in that a sharp and stiff corner forms in the simulation while it collapses rapidly in the experiments. This discrepancy may be due to the rapid decrease of the solid volume fraction at the corner. As we know, during the collapse process, a vortex forms at the corner. Under the action of the vortex, solid particles are eroded and solid volume fraction decreases, leading to more pronounced collapse at the corner. Using constant internal friction angle and hydraulic conductivity, as did in the present study, might not be able to describe such complex interactions between water and solid at the corner. It is noted that the numerical simulation of Savage et al. [11] using FEM demonstrates a similar behavior as that obtained in our simulation. Thus, modeling dense granular column collapse remains a big challenge. Despite some discrepancies, the proposed SPH approach is able to predict the slow regime of the dense granular column collapse.

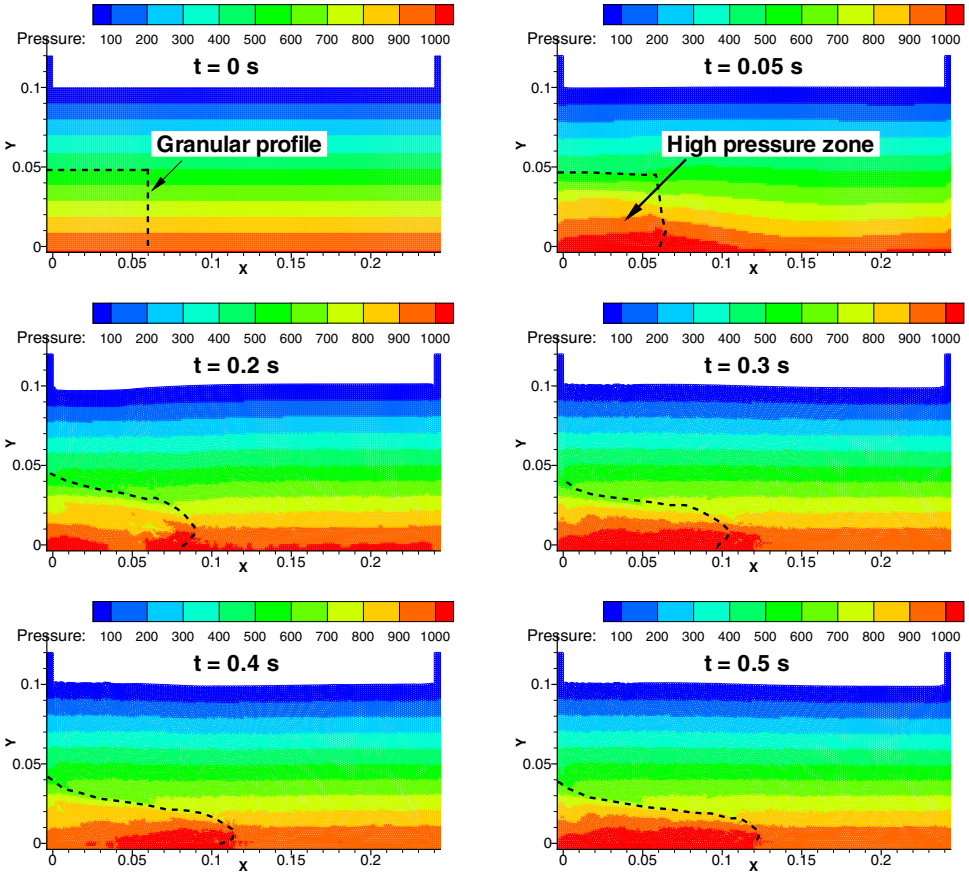

Fig. 5. Pressure field during the collapse process of loose packing.

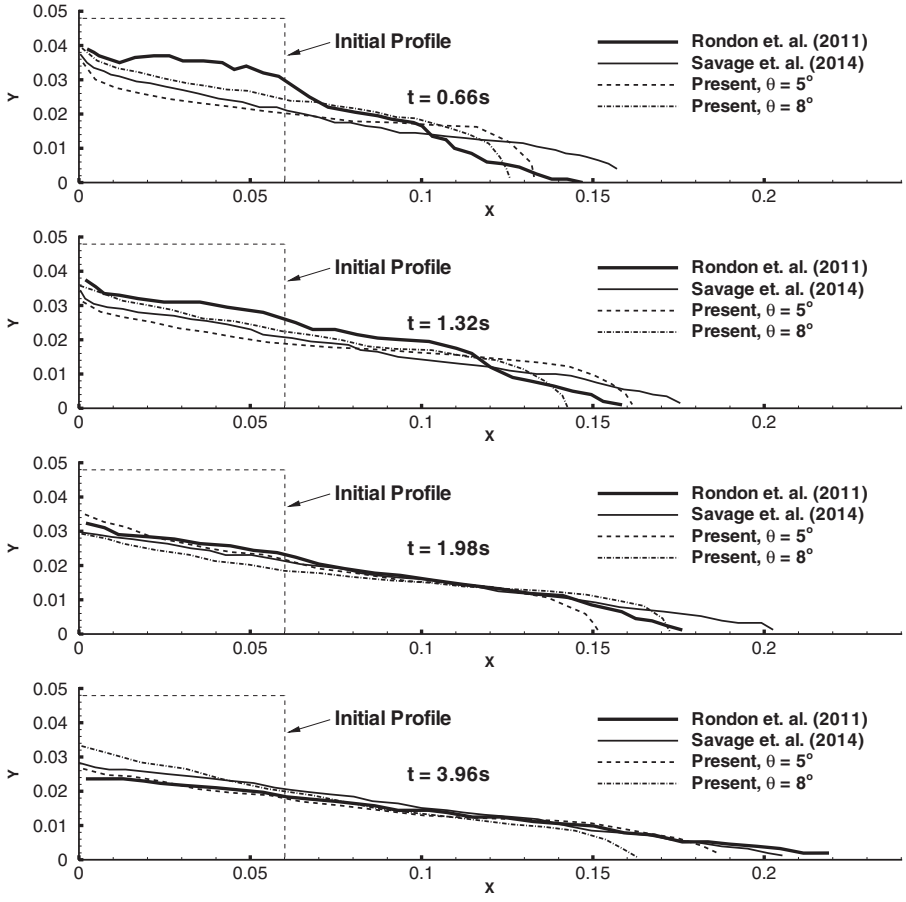

Fig. 6. Deposit profiles at different times for submerged loose packing granular column collapse.

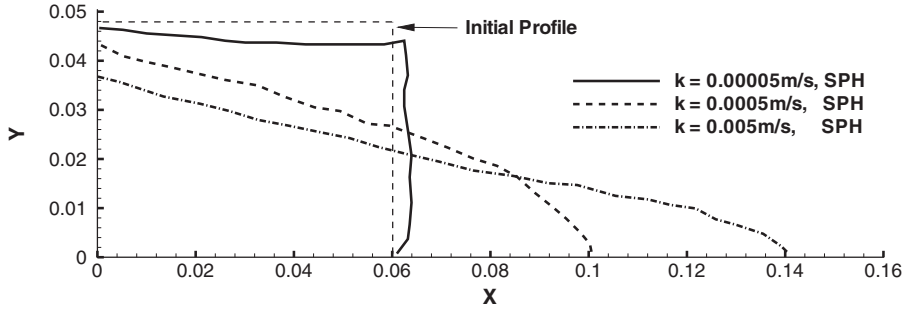

Fig. 7. Influence of hydraulic conductivity k on the deposit profile at $t = 2$ s, in case of $\theta = 25^{\circ}$.

Fig. 9 shows the water pressure field at some representative times. It can be seen that at the initial stage of the collapse, a low pressure zone is formed inside the granular column, due to the dilation occurred when granular material is subjected to shearing. On the contrary, a high pressure zone is formed at the toe of the column where water is displaced by the grains. As a result of the dilation, the interstitial pore volume is increased giving rise to a negative pore pressure and fluid is drawn into the interstitial space. Here, again, "negative" means the pressure is lower than the hydrostatic counterpart of the surrounding fluid at the same depth. As the fluid flows into the negative pore-pressure region, the negative pore-pressure subsides and the interstitial fluid pressure increases to restore that of the surrounding water during the collapse development. However, we have to point out that long time simulation for dense granular column collapse is very time consuming, thus the final stoppage of the collapse and the fully restoration of the pressure to the hydrostatic case are rarely achieved in our computation.

Finally, to demonstrate the capability of the present SPH model in dealing with granular flows, we simulate several granular column collapses and investigate the runout distances under different aspect ratios. The analysis of the runout can be reduced to the measurement of the apparent slope H_f/L_f of the deposit, where H_f and L_f are the final height and length of the deposit respectively. Fig. 10 shows how the apparent slope H_f/L_f varies with respect to the initial aspect ratio H_i/L_i for granular column collapses in dry, loose and dense packing and compares our simulation results with the experimental data of Rondon et al. [8]. It can be seen that the collapse of a dense packing column results in a steep slope, while for the loose case the slope is much smaller. The dry column collapse exhibits a medium slope. Thus the ambient fluid has important influences on the morphology of the submerged granular column collapse.

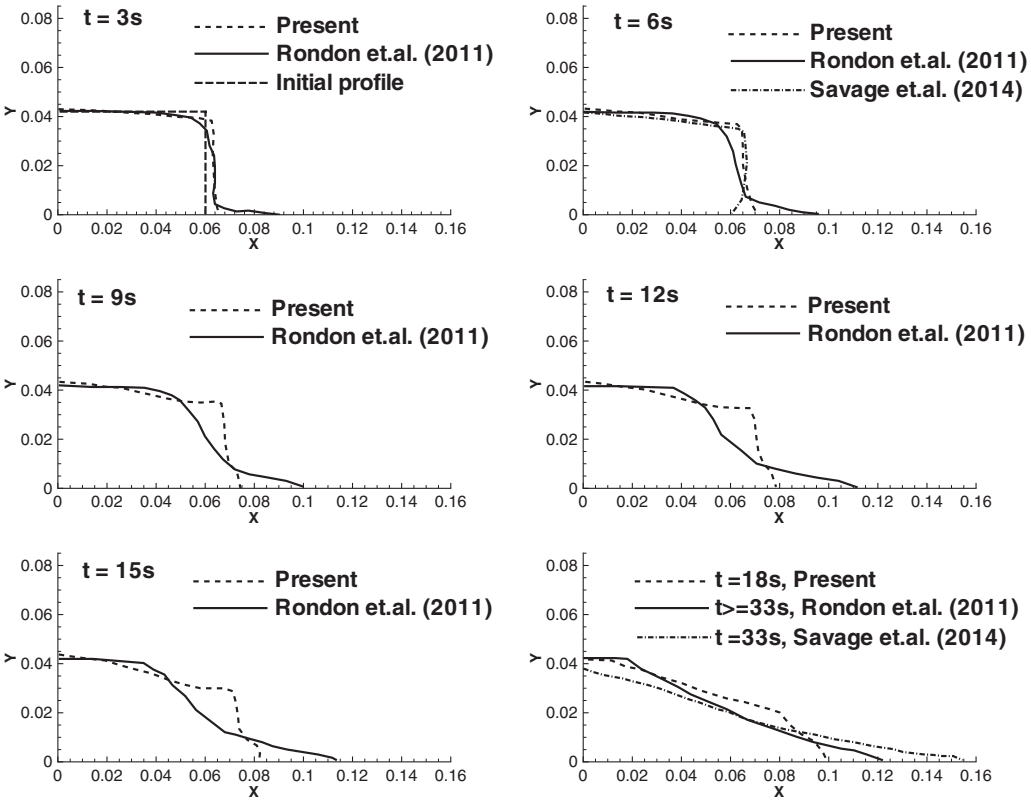

Fig. 8. Deposit profiles of dense granular column collapse at different times, in case of $\theta = 25^{\circ}$, $k = 0.00005$ m/s.

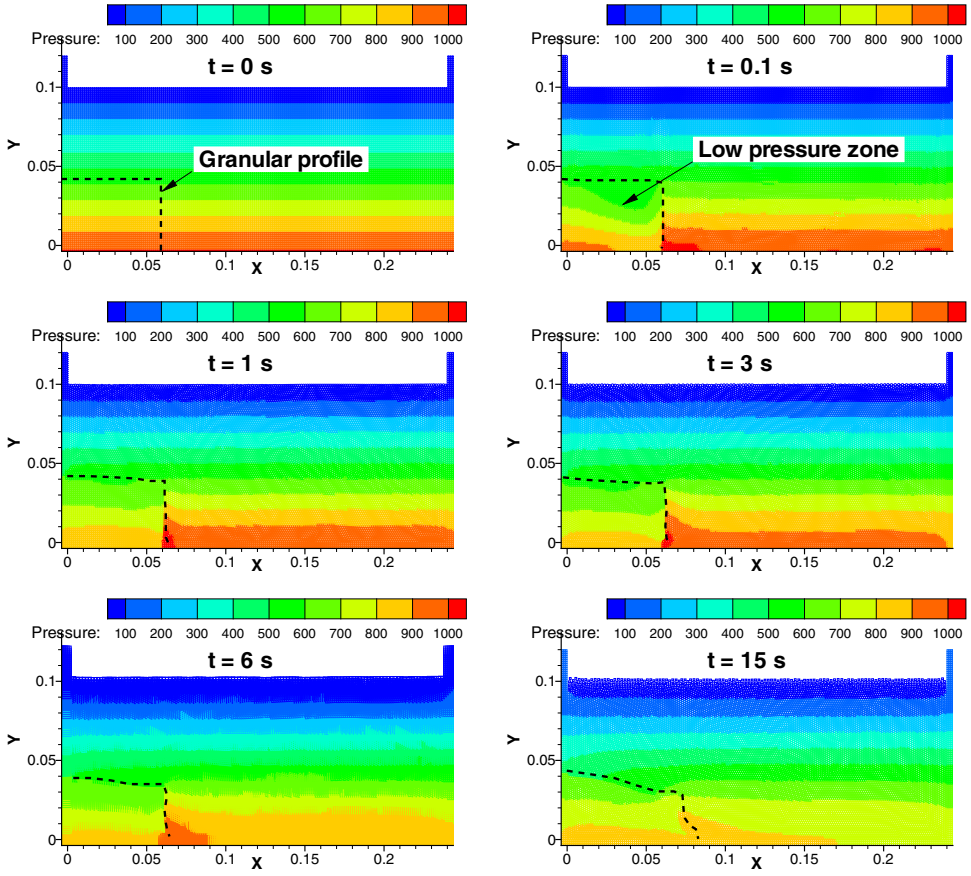

Fig. 9. Pressure field during the dense granular column collapse.

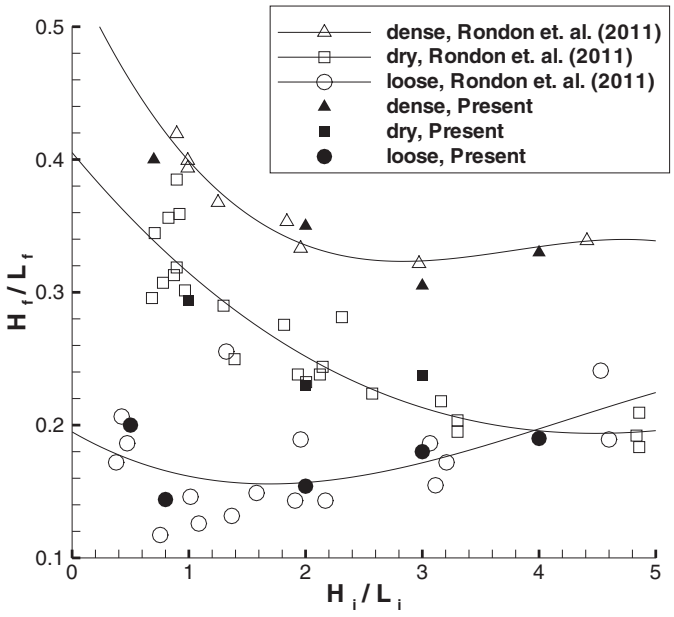

Fig. 10. Apparent slope H_f/L_f as a function of initial aspect ration H_i/L_i for loose, dense and dry column collapses.

For all the cases, our numerical simulation recovers experimental observations of Rondon et al. [8] with good satisfaction.

5. Conclusions

In this paper, numerical simulation of submerged granular column collapse by means of two-fluid mixture smoothed particle hydrodynamics method (SPH) is presented. Two regimes of the collapse, one being quick and the other being slow, could be seen from the simulation. The internal friction angle and hydraulic conductivity of the solid particles play important roles in the formation of different regimes. For small internal friction angle, the collapse process takes seconds; whereas large friction angle can retard the flow significantly. The hydraulic conductivity is also a key factor to the collapse. In case of large conductivity, the water flows through the granular material easily, leading to a rapid collapse process; while for small conductivity, the collapse takes much longer time. Agreement between our results and other researchers' numerical and experimental results is good, which illustrates the capability of the proposed two-fluid SPH approach in studying the complex interactions between water and solid particles in saturated mixture flows.

Although our numerical simulations agree with the experimental observations and the numerical simulations of other researchers, more comprehensive and detailed investigations of the phenomenon are still needed. For example, the compaction of a loose packing is mimicked here by the reduced internal friction angle. It is true that the dilatancy angle is dynamical according to the critical state theory, i.e. it changes value during the collapse process. In the current study, however, we adopt a constant dilatancy angle and find that it gives acceptable results in many cases. We point out that for a good recovery of the experimental observations, a subtle incorporation of the dilatancy angle should be considered. An SPH method combined with the rigorous critical state theory may be appropriate to predict the collapse more accurately. In addition, the assumption of a constant hydraulic conductivity allows obtaining reasonable results from an engineering point of view, as shown in this paper. However, theoretically speaking, the hydraulic conductivity should be influenced by the mechanical deformation of the soil, thus a hydraulic conductivity variable with the porosity may be attempted to get more accurate predictions of the collapse.

Acknowledgement

This work is partly supported by the National Key Basic Research Program of China (Approval No. 2014CB046801).

References

[1] R.M. Iverson, The physics of debris flows, Rev. Geophys. 35 (1997) 245–296.
[2] F. Legros, The mobility of long-runout landslides, Eng. Geol. 63 (2002) 301–331.
[3] M.A. Hampton, H.J. Lee, J. Locat, Submarine landslides, Rev. Geophys. 34 (1996) 33–59.
[4] P. Jop, Y. Forterre, O. Pouliquen, A constitutive law for dense granular flows, Nature 441 (2006) 727–730.
[5] Y. Forterre, O. Pouliquen, Flows of dense granular media, Annu. Rev. Fluid Mech. 40 (2008) 1–24.
[6] P.-Y. Lagree, L. Staron, S. Popinet, The granular column collapse as a continuum: validity of a two-dimensional Navier–Stokes model with a $\mu(I)$-rheology, J. Fluid Mech. 686 (2011) 378–408.
[7] I.R. Ionescu, A. Mangeney, F. Bouchut, O. Roche, Viscoplastic modeling of granular column collapse with pressure-dependent rheology, J. Non-Newton. Fluid Mech. 219 (2015) 1–18.
[8] L. Rondon, O. Pouliquen, P. Aussillous, Granular collapse in a fluid: role of the initial volume fraction, Phys. Fluids 23 (2011) 073301.
[9] C. Meruane, A. Tamburrino, O. Roche, On the role of the ambient fluid on gravitational granular flow dynamics, J. Fluid Mech. 648 (2010) 381–404.
[10] C. Meruane, A. Tamburrino, O. Roche, Dynamics of dense granular flows of small-and-large-grain mixtures in an ambient fluid, Phys. Rev. E 86 (2012) 026311.
[11] S. Savage, M. Babaei, T. Dabros, Modeling gravitational collapse of rectangular granular piles in air and water, Mech. Res. Commun. 56 (2014) 1–10.
[12] H.H. Bui, K. Sako, R. Fukagawa, Numerical simulation of soil–water interaction using smoothed particle hydrodynamics (SPH) method, J. Terramech. 44 (2007) 339–346.
[13] H.H. Bui, R. Fukagawa, K. Sako, S. Ohno, Lagrangian meshfree particles method (SPH) for large deformation and failure flows of geomaterial using elastic-plastic soil constitutive model, Int. J. Numer. Anal. Methods Geomech. 32 (2008) 1537–1570.
[14] H.H. Bui, R. Fukagawa, An improved SPH method for saturated soils and its application to investigate the mechanisms of embankment failure: case of hydrostatic pore-water pressure, Int. J. Numer. Anal. Methods Geomech. 37 (2013) 31–50.
[15] C. Peng, W. Wu, H.-S. Yu, C. Wang, A SPH approach for large deformation analysis with hypoplastic constitutive model, Acta Geotech. 10 (2015) 703–717.
[16] S. Dunatunga, K. Kamrin, Continuum modelling and simulation of granular flows through their many phases, J. Fluid Mech. 779 (2015) 483–513.
[17] X. Zhang, K. Krabbenhoft, D. Pedroso, A. Lyamin, D. Sheng, M.V. da Silva, D. Wang, Particle finite element analysis of large deformation and granular flow problems, Comput. Geotech. 54 (2013) 133–142.
[18] C. Wang, Y. Wang, C. Peng, X. Meng, Smoothed particle hydrodynamics simulation of water–soil mixture flows, J. Hydraul. Eng. 142 (2016) 04016032.
[19] S. Zhang, C. Wang, T. Ge, Experimental prediction of the noncontact jet trencher's excavation depth in clay, Mar. Georesour. Geotechnol. 35 (2017) 300–304.
[20] S. Zhang, M. Zhao, T. Ge, C. Wang, Experimental research on trenching in stiff clay by submerged vertical traveling jets, J. Coast. Res. 32 (2016) 365–373.
[21] X. Meng, Y. Wang, Modelling and numerical simulation of two-phase debris flows, Acta Geotech. 11 (2016) 1027–1045.
[22] J. Gray, A. Thornton, A theory for particle size segregation in shallow granular free-surface flows, Proc. R. Soc. A: Math. Phys. Eng. Sci. 461 (2005) 1447–1473.
[23] W.F. Chen, E. Mizuno, Nonlinear Analysis in Soil Mechanics: Theory and Implementation, Elsevier, Amsterdam, 1990.
[24] J.J. Monaghan, A. Kocharyan, SPH simulation of multi-phase flow, Comput. Phys. Commun. 87 (1995) 225–235.
[25] J.J. Monaghan, Implicit SPH drag and dusty gas dynamics, J. Comput. Phys. 138 (1997) 801–820.
[26] J.J. Monaghan, Simulating free surface flows with SPH, J. Comput. Phys. 110 (1994) 399–406.
[27] M. Pailha, O. Pouliquen, A two-phase flow description of the initiation of underwater granular avalanches, J. Fluid Mech. 633 (2009) 115–135.
[28] M. Pailha, M. Nicolas, O. Pouliquen, Initiation of underwater granular avalanches: influence of the initial volume fraction, Phys. Fluids 20 (2008).
[29] B. Andreotti, Y. Forterre, O. Pouliquen, Granular Media: Between Fluid and Solid, Cambridge University Press, 2013.
[30] S. Roux, F. Radjai, Texture-dependent rigid-plastic behavior, in: Physics of Dry Granular Media, Springer, 1998, pp. 229–236.